Experimental Investigation of Effects of Di-N-Butyl Ether Addition on Spray Macroscopic Characteristics of Diesel-Biodiesel Blends

Yanju Liu[1]; Fengyu Li, Ph.D.[2]; Wei Fu, Ph.D.[3]; Xuedan Jiang[4]; Zhihui Song[5]; Zuojin Zhu[6]; and Qizhao Lin[7]

Abstract: Di-n-butyl ether (DBE) is one of the most promising alternative biofuels for vehicles due to its superior physicochemical properties and because it is a renewable resource. This study investigated the effects of DBE addition on the spray macroscopic characteristics of diesel-biodiesel blends under various injection and ambient conditions. Three kinds of ternary blended fuels were prepared—(1) 72% diesel, 18% biodiesel, 10% DBE by volume (D72B18DBE10); (2) 64% diesel, 16% biodiesel, 20% DBE by volume (D64B16DBE20); and (3) 56% diesel, 14% biodiesel, and 30% DBE by volume (D56B14DBE30)—in order to compare their spray characteristics with those of an 80% diesel–20% biodiesel mix (D80B20) and conventional diesel (D100). The experiments were conducted in a constant volume chamber with a high-pressure common rail injection system using a high-speed photography method. The results show that D80B20 gives the longest spray tip penetration and the smallest cone angle and projected area among the five test fuels. With increased DBE blending ratio, the spray penetration length decreases slightly, and spray cone angle and projected area increase. When the DBE volume fraction in the ternary blend is 20%, the spray tip penetration, cone angle, and projected area are comparable to those of diesel. In addition, air entrainment characteristics were analyzed with the quasi-steady jet theory. It was found that the addition of DBE can improve the air entrainment characteristics of diesel-biodiesel blends, and D64B16DBE20 results in fuel-air mixing similar to that of D100. **DOI: 10.1061/(ASCE)EY.1943-7897.0000630.**

Author keywords: Diesel; Biodiesel; Di-n-butyl ether; Spray characteristics.

Introduction

The application of renewable fuels as alternatives or additives to conventional fossil fuels for vehicles is considered to be an effective method of responding to the energy crisis and strict emission standards. On the one hand, according to British Petroleum's (BP) statistical review of world energy in 2017, global primary energy consumption growth remained strong. China accounted for 33.6% of global energy consumption growth in 2017 and was the largest contributor to global growth for 17 consecutive years. Moreover, China's oil import dependency ratio rose to 68% in 2017, the highest in its history (BP 2017). Although fossil fuels will remain dominant for the next 65 years (Huang et al. 2012), China will inevitably face a huge energy crisis and a severe energy security challenge. On the other hand, various emissions such as hydrocarbons (HC), carbon monoxide (CO), nitrogen oxides (NOx) and particulate matter (PM) are produced by the combustion of fossil fuels, causing environmental pollution and climate change (Park et al. 2015; Vardy et al. 2017; Coram and Katzner 2018). Faced by these challenges, many researchers have investigated clean, renewable, and alternative fuels, such as hydrogen (Krishnan et al. 2014), natural gas (Sajjad et al. 2014), alcohol fuels (Szybist et al. 2011; Zhen and Wang 2015; Li et al. 2017; Yi et al. 2017; Belgiorno et al. 2018; Wang et al. 2018), ethers (Park and Lee 2013), and esters (Boggavarapu and Ravikrishna 2013). Among these, biodiesel (a kind of ester) has been widely studied as a fuel substitute for mineral diesel because of its degradability, nontoxicity, and having physicochemical properties similar to diesel.

Specifically, Suresh et al. (2018) reported on the combustion, performance, and emission characteristics of biodiesel refined from nonedible oils and on the performance of biodiesel blends in variable compression ratio (VCR) diesel engines. They pointed out that burning biodiesel in VCR engines resulted in an increased heat release rate at the late of combustion and lower ignition delay period than mineral diesel. Regarding engine performance, they found enhanced brake thermal efficiency, decreased brake power, and increased mechanical efficiency at higher compression ratios. They also showed that reduced emissions of carbon dioxide (CO_2), carbon monoxide, sulfur oxides (SOx), and smoke were achieved by using biodiesels rather than diesel. Lapuerta et al. (2008) pointed

[1]Master's Candidate, Dept. of Thermal Science and Energy Engineering, Univ. of Science and Technology of China, No. 96, Jinzhai Rd., Hefei, Anhui 230026, PR China. Email: yjstar@mail.ustc.edu.cn

[2]Dept. of Thermal Science and Energy Engineering, Univ. of Science and Technology of China, No. 96, Jinzhai Rd., Hefei, Anhui 230026, PR China. Email: lfy1995@mail.ustc.edu.cn

[3]Dept. of Thermal Science and Energy Engineering, Univ. of Science and Technology of China, No. 96, Jinzhai Rd., Hefei, Anhui 230026, PR China. Email: fw123@mail.ustc.edu.cn

[4]Master's Candidate, Dept. of Thermal Science and Energy Engineering, Univ. of Science and Technology of China, No. 96, Jinzhai Rd., Hefei, Anhui 230026, PR China. Email: jxd95@mail.ustc.edu.cn

[5]Master's Candidate, Dept. of Thermal Science and Energy Engineering, Univ. of Science and Technology of China, No. 96, Jinzhai Rd., Hefei, Anhui 230026, PR China. Email: szhihui@mail.ustc.edu.cn

[6]Associate Professor, Dept. of Thermal Science and Energy Engineering, Univ. of Science and Technology of China, No. 96, Jinzhai Rd., Hefei, Anhui 230026, PR China. Email: zuojin@ustc.edu.cn

[7]Professor, Dept. of Thermal Science and Energy Engineering, Univ. of Science and Technology of China, No. 96, Jinzhai Rd., Hefei, Anhui 230026, PR China (corresponding author). ORCID: https://orcid.org/0000-0003-2572-2811. Email: qlin@ustc.edu.cn; 18255107780@163.com

Note. This manuscript was submitted on November 12, 2018; approved on March 29, 2019; published online on September 28, 2019. Discussion period open until February 28, 2020; separate discussions must be submitted for individual papers. This paper is part of the ***Journal of Energy Engineering***, © ASCE, ISSN 0733-9402.

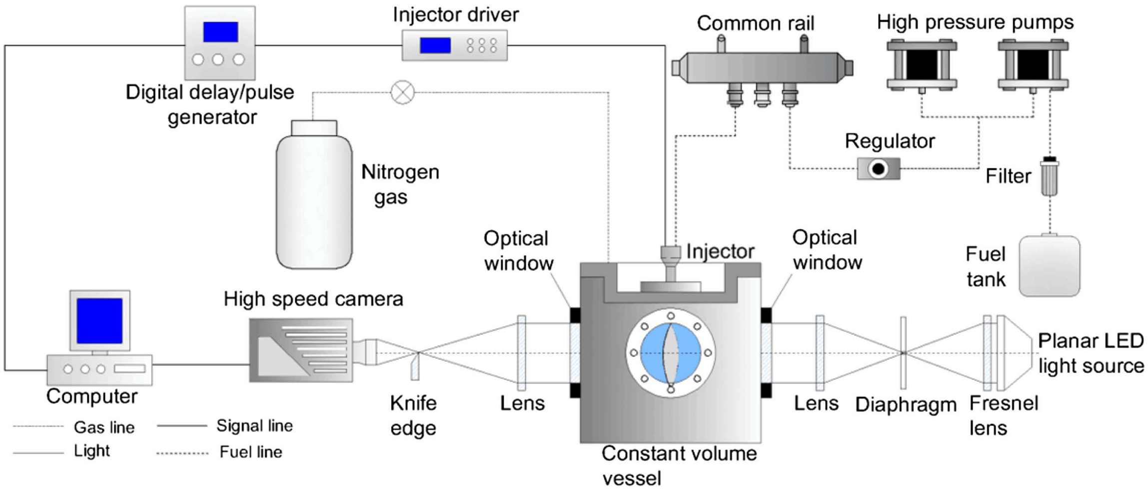

Fig. 1. Schematic of the experimental setup.

out that total hydrocarbon (THC) emissions and the mean diameter of particle size distributions (PSDs) were reduced when using biodiesel fuel. Dhar and Agarwal (2014) indicated that the maximum torque attained using Karanja biodiesel (KOME) blends in a direct injection compression ignition (DICI) engine was higher than that attained using mineral diesel, and the brake specific fuel consumption (BSFC) for KOME blends was equal to that of basal diesel.

However, there are several issues with regard to the practical application of biodiesel. First, it is not economical to burn neat biodiesel in engines. In general, biodiesel is produced by transesterifying vegetable/plant oils, animal oils, waste oils, or microbial oils with low-molecular-weight alcohols (Knothe and Razon 2017). The cost of its feedstock, such as vegetable oils, or the costs involved in extra steps for pretreatment of cheaper but less valuable feedstock are rather high (Akgün and İşcan 2007; Gebremariam and Marchetti 2018), making biodiesel less economical. In addition, in order to acquire the same power, a surplus in fuel consumption is required because of biodiesel's lower calorific value than

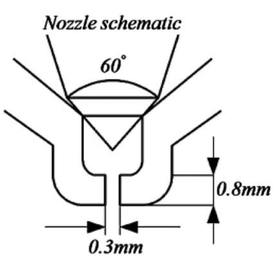

Fig. 2. Structure of the injector nozzle.

Table 2. Test conditions

Test conditions	Values
Test fuels	D100, D80B20, D72B18DBE10, D64B16DBE20, D56B14DBE30
Injection pressure (MPa)	60, 70, 80, 90, 100
Ambient pressure (MPa)	1, 2, 3
Ambient temperature (K)	298
Energizing time (μs)	700
Nozzle type	Minisac nozzle
Hole number	Single hole

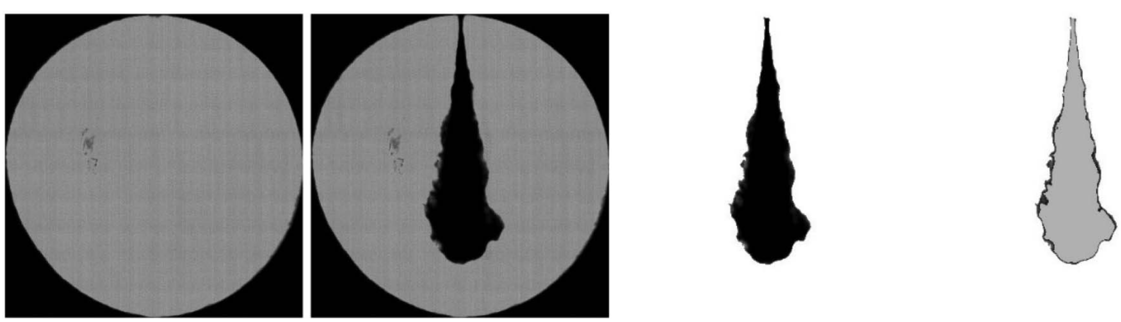

Fig. 3. Spray image processing procedure.

Table 1. Test fuels

Properties	D100	D80B20	D72B18DBE10	D64B16DBE20	D56B14DBE30
Density (25°C) (kg/m^3)	823.26	860.22	851.42	841.02	814.16
Viscosity (25°C) (mm^2/s)	2.67	2.89	2.36	1.99	1.86

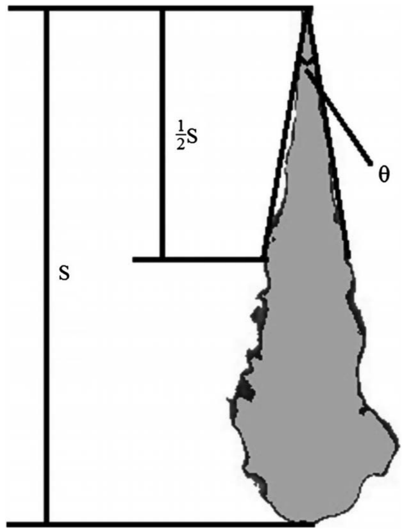

Fig. 4. Definition of the spray macroscopic characteristic parameters.

diesel (Boggavarapu and Ravikrishna 2013). Moreover, compared with mineral diesel, the higher pour point and viscosity and lower volatility of biodiesel cause deteriorated engine cold start performance (Zare et al. 2018). Consequently, biodiesel has usually been used as an additive to mineral diesel in previous studies (Dhar and Agarwal 2014; Xie et al. 2015; Zhan et al. 2018). Its higher surface tension and viscosity result in inferior spray and atomization characteristics for biodiesel blends than for mineral diesel under the same operating conditions; this, in turn, is expected to worsen the quality of the fuel-air mixture and further reduce engine combustion efficiency. Das et al. (2018) tested the spray characteristics of three types of diesel-biodiesel blends (DB) and found that the addition of biodiesel led to larger mean droplet size and narrower cone angle than were found for basal diesel alone. Some studies (Dhar et al. 2012; Boggavarapu and Ravikrishna 2013) have indicated that it is necessary to redesign and optimize the engine components when using diesel-biodiesel blends in diesel engines because of the different spray characteristics of diesel-biodiesel blends. However, adding other biofuels with excellent physicochemical properties may be effective in ameliorating the worsening of spray characteristics, thereby improving emission and combustion characteristics.

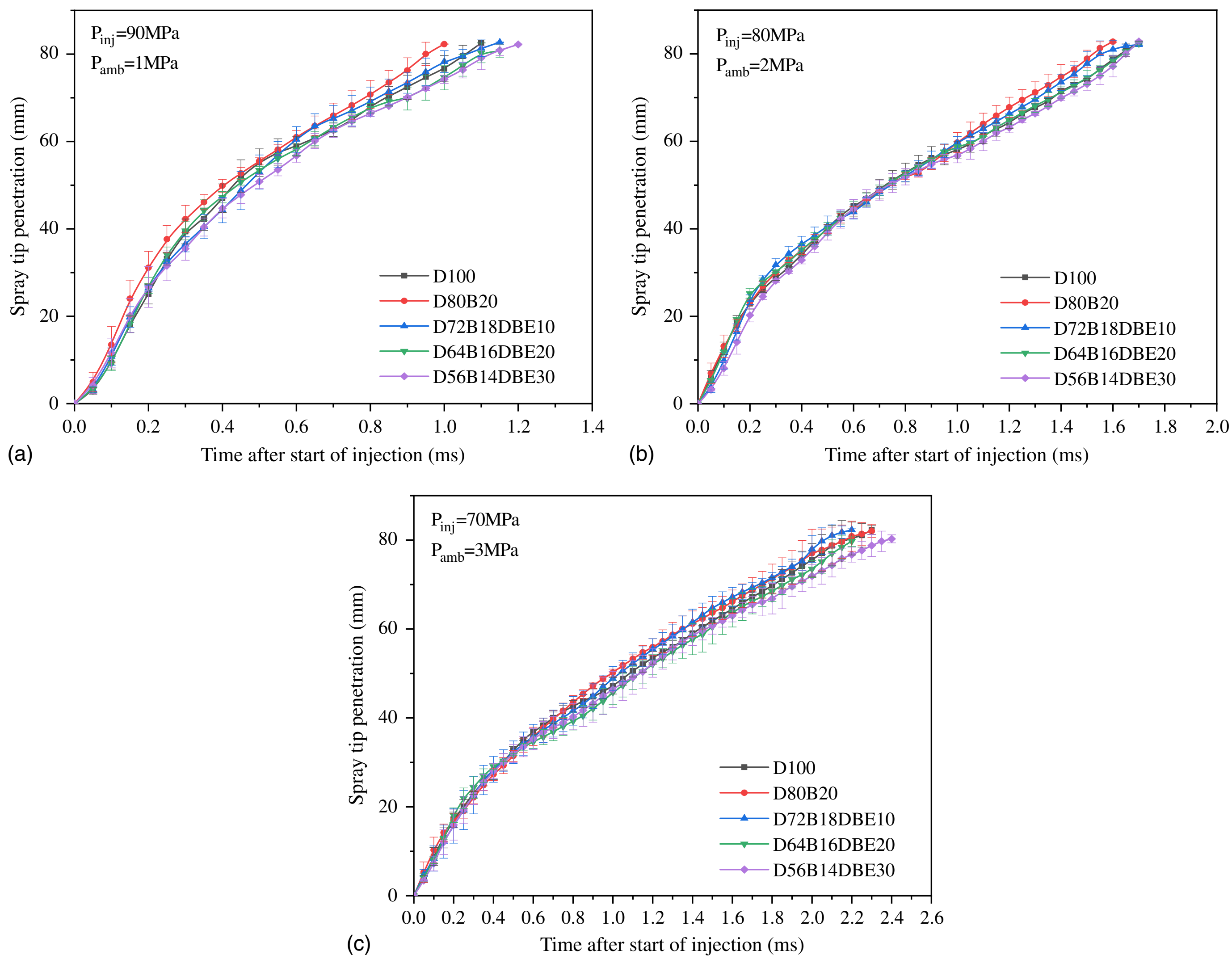

Fig. 5. Spray tip penetration for diesel and blended fuels under (a) injection pressure of 90 MPa and ambient pressure of 1.0 MPa; (b) injection pressure of 80 MPa and ambient pressure of 2.0 MPa; and (c) injection pressure of 70 MPa and ambient pressure of 3.0 MPa.

An experiment in a single cylinder compression ignition engine with diesel-biodiesel-ethanol blends was conducted by Shamun et al. (2018). The results showed that the addition of ethanol made the efficiency and emissions of the blends as good as or superior to those of conventional diesel. However, the effects of the addition of di-n-butyl ether on the spray macroscopic characteristics of diesel-biodiesel blends have been less explored.

Di-n-butyl ether (DBE), a linear C_8-oxygenate, has been identified as an ideal potential biofuel candidate for compression ignited (CI) engines (Bi et al. 2009). It can be produced through the dehydration of n-butanol, which is available from biomass waste containing lignocellulose (L. E. Manzer, M. B. D'Amore, E. S. Miller, and J. P. Knapp, "Process for making dibutyl ethers from dry 2-butanol," Google Patent No. 2008O132734A1 (2008); Wullenkord et al. 2018). Therefore, it is a second-generation biofuel that does not threaten the food chain. In addition, DBE has appealing properties. The cetane number of DBE is higher than that of biodiesel and diesel, which improves autoignition performance. Considering its higher evaporation latent heat, the addition of DBE is expected to reduce the maximum temperature during the combustion process and ultimately influence emissions performance. Compared to diesel, the application of DBE in a single-cylinder engine caused a decrease in overall hydrocarbon, carbon monoxide, and soot emissions (Heuser et al. 2015). The results from Miyamoto's experiment (Miyamoto et al. 2000) proved that NOx was reduced when using DBE in a single-cylinder four-stroke-cycle diesel engine. DBE has a higher vapor pressure and lower boiling point than diesel, indicating that the volatility of DBE is better; this is beneficial for mixture formation. The viscosity and surface tension of DBE are lower than those of diesel; this is beneficial for spray and atomization performance (Meng et al. 2008; Bi et al. 2009). The spray structures of DBE alone and its blends with diesel showed improved spray and atomization processes (Beeckmann et al. 2010; Guan et al. 2015; Zhan et al. 2018).

It is well known that the combustion process, which affects final engine performance and emission levels, is primarily dominated by the quality of the fuel-air mixture. The effects of the addition of di-n-butyl ether on the spray and atomization processes of diesel-biodiesel blends remain unknown. Therefore, DBE was added to diesel-biodiesel blends at different volume fractions in order to investigate whether DBE can improve the spray characteristics of DBs and make the fuel-air mix similar to that of diesel without any modifications to the diesel engine. The addition of DBE will also increase the renewable fraction of the blends. The proportion of biodiesel added to diesel is usually less than 20% (Dhar and Agarwal 2014; Zhan et al. 2018). In this study, the blending ratio

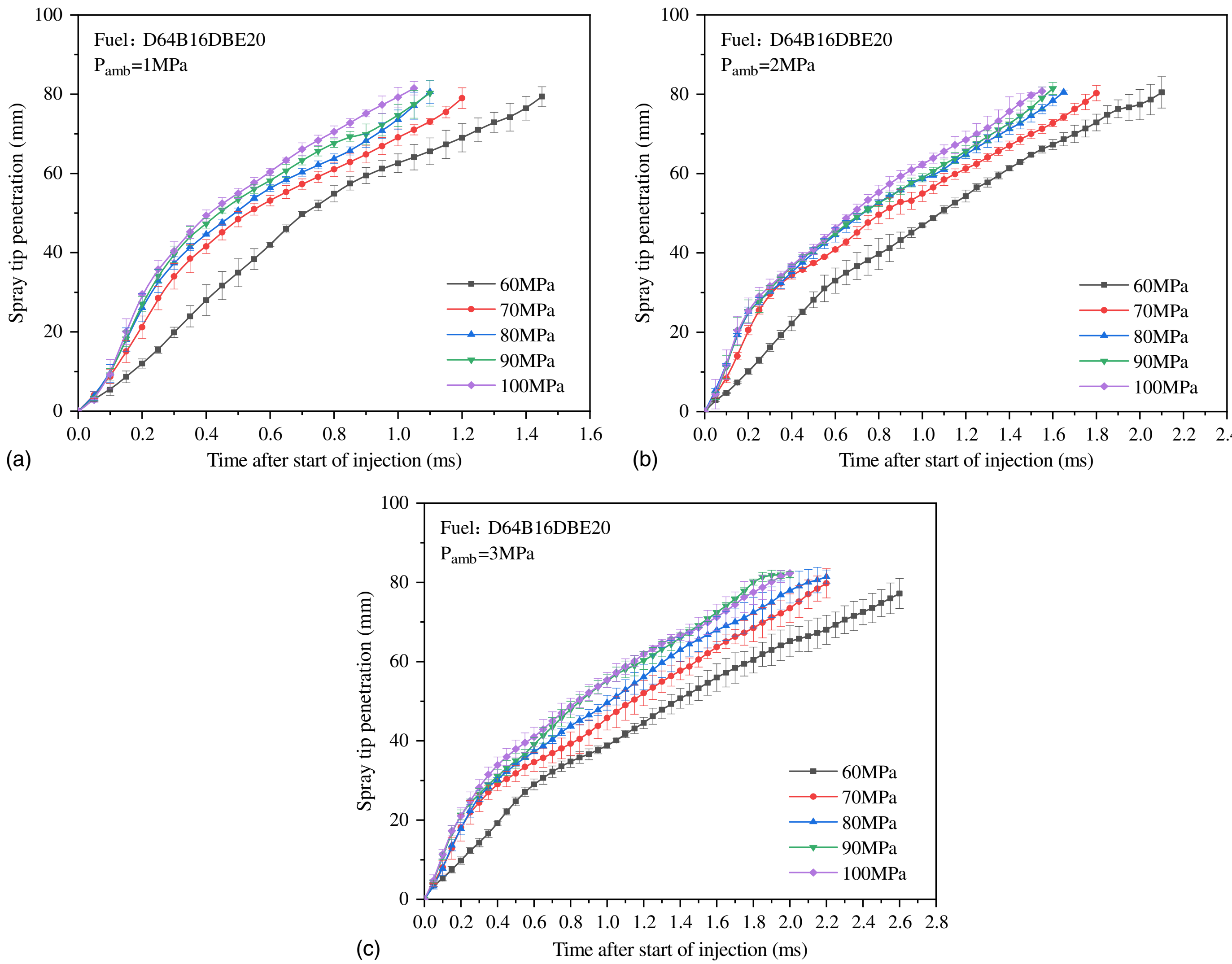

Fig. 6. Effect of injection pressure on spray tip penetration of D64B16DBE20 under ambient pressure of (a) 1.0 MPa; (b) 2.0 MPa; and (c) 3.0 MPa.

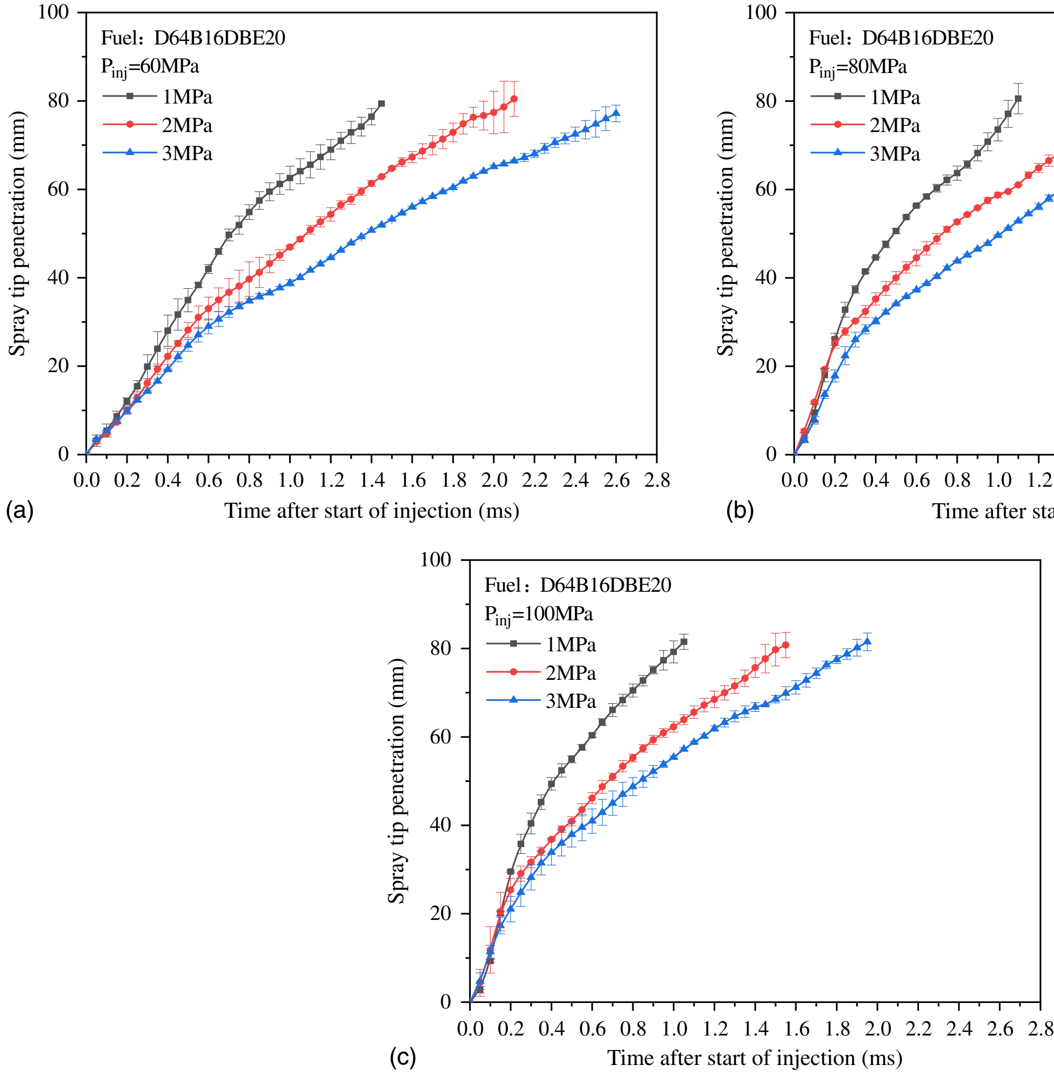

Fig. 7. Effect of ambient pressure on spray tip penetration of D64B16DBE20 under injection pressure of (a) 60 MPa; (b) 80 MPa; and (c) 100 MPa.

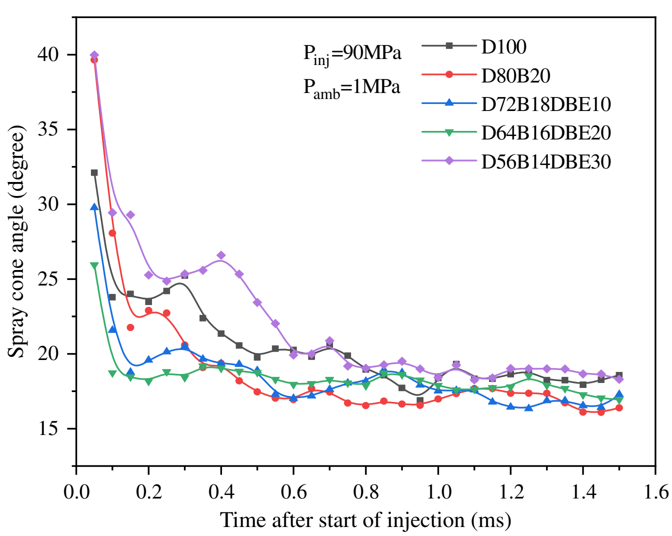

Fig. 8. Spray cone angle for diesel and blended fuels at injection pressure of 90 MPa and ambient pressure of 1 MPa.

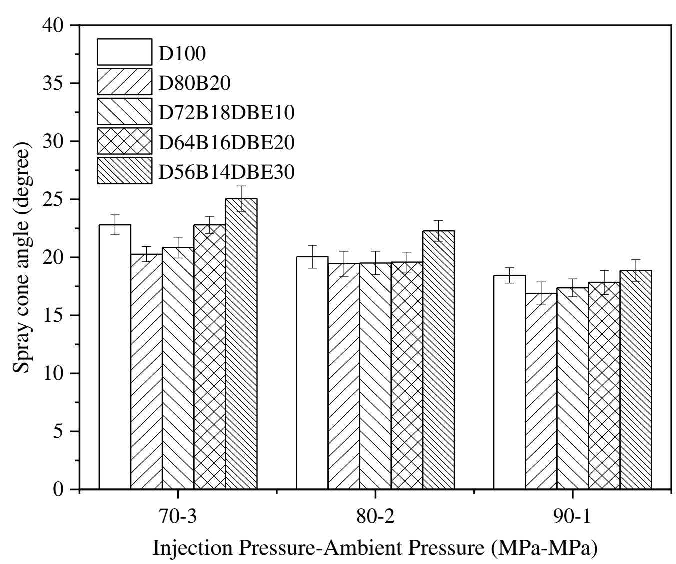

Fig. 9. Time-averaged spray cone angle for diesel and blended fuels.

of biodiesel in the diesel-biodiesel blend will be 20%. In this study, in combination with the effects on the combustion engine, the spray macroscopic characteristics for conventional diesel (D100), an 80% diesel–20% biodiesel blend (D80B20), and three ternary blends were studied in detail under various injection and ambient conditions; studied characteristics included spray tip penetration, spray cone angle, and spray projected area. In addition, the effects of DBE blending ratio and ambient pressure (P_{amb}) on the equivalence ratio calculated by previous formulas will be discussed.

Experimental Setup and Procedure

Apparatus and Procedure

As shown in Fig. 1, the experimental setup used in this study mainly consisted of three parts: the fuel-injection facility, the constant volume chamber, and the high-speed photography system.

The fuel-injection facility was employed to generate high pressure fuels. The test fuel was pumped through the filter, high pressure pumps, and regulator in turn, fed into the common rail, and then injected into the constant volume chamber through a Bosch common-rail injector [(Model No. 0445120224 (Stuttgart, Germany)], which was controlled by a solenoid valve. The energizing time was set to 700 μs. Fig. 2 shows details of the single hole nozzle with diameter of 0.3 mm. The injection pressure (P_{inj}) was adjusted and monitored by the high pressure common-rail system with an accuracy of $\pm$1.6%.

The constant volume chamber was made of stainless steel, and two round quartz windows with a diameter of 80 mm were installed on opposite sides for the spray visualization. The constant volume chamber was filled with nitrogen gas supplied by compressed nitrogen bottles to simulate high-pressure conditions (able to withstand pressures up to 12 MPa). Various ambient pressures were obtained by manually adjusting the intake and exhaust valves mounted on the chamber, and the pressure was measured and displayed by a pressure gauge installed on the constant volume chamber.

The high-speed photography system was comprised of a continuous 180-watt light-emitting diode (LED) light source, two lenses (for producing parallel light and collecting light, respectively), a high-speed camera (Fastcam SA5 1000K-M3, Photron, Tokyo), and a data acquisition and processing device. In this study, the schlieren technique was used to investigate the spray macroscopic characteristics. The high-speed camera captured transient spray images at a rate of 20,000 frames per second (fps) with an exposure time of 1/20,000 s. The trigger signals of the camera

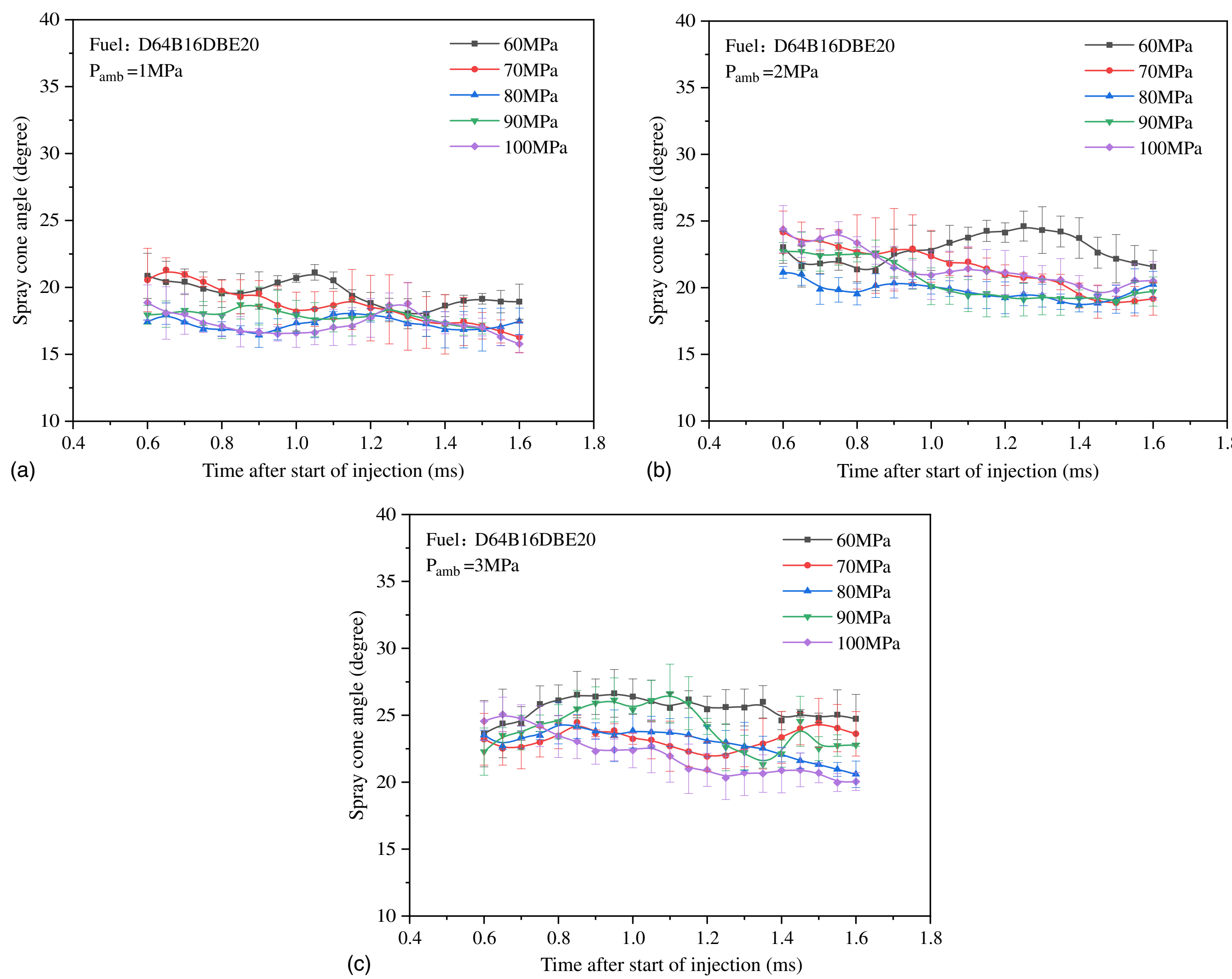

Fig. 10. Effect of injection pressure on spray cone angle of D64B16DBE20 under ambient pressure of (a) 1.0 MPa; (b) 2.0 MPa; and (c) 3.0 MPa.

and the injector were synchronized by a digital delay/pulse generator. Because the spray tip reached the bottom of the optical window within 3 ms after the start of injection, the duration of the photography of the spray process was set to 3 ms in order to record the complete spray images.

In order to obtain quantitative spray parameters, the captured spray images were first processed. Fig. 3 shows the typical spray image processing procedure. First, a background image was prerecorded and stored before the start of injection, with no spray present. Second, the spray images were subtracted from the stored background image, and a fixed gray threshold value was chosen. Third, all spray evolution images were processed according to the threshold value, and contour images were determined. Last, spray macroscopic characteristic parameters were measured using the contour images by scaling the pixels to real linear scale.

Test Fuels and Conditions

Five kinds of fuels were tested in this study, as shown in Table 1. Commercial #0 diesel was used as the basal fuel. Soybean biodiesel and DBE with a purity of 99% were purchased from COFCO, Tianjin, China and Shanghai Macklin Biochemical, Shanghai, China, respectively. As mentioned previously, the most frequently used volume blending ratio for biodiesel in diesel is no more than 20%. Thus, a mixture (D80B20) composed of 80% diesel and 20% soybean biodiesel (by volume) was prepared. The other three ternary blends were then obtained by blending DB with 10%, 20%, and 30% DBE, respectively. It is remarkable that in order to compare the effects of the addition of DBE on the spray macroscopic characteristics of DB, the ratio of diesel to biodiesel remained unchanged (4:1) in this work. Ternary blends can be stable (Shamun et al. 2018). In this study, none of the diesel–biodiesel–DBE blends separated within two weeks or during the test campaign, demonstrating that the blends were stable. The fuel density was calculated by dividing the fuel mass by the volume; the kinematic viscosity was measured by a kinetic viscometer (Type SYD-265H, Shanghai Changji, China). As Table 1 shows, the density and viscosity of D80B20 were the largest among the five fuels; these two parameters decreased as the volume fraction of DBE in the DB increased.

Five injection pressures (60, 70, 80, 90, and 100 MPa) and three ambient pressures (1, 2, and 3 MPa) were adopted. The ambient temperature was room temperature (298 K). Detailed test conditions are listed in Table 2. To ensure the reliability of the experimental results, the tests were repeated three times under each condition.

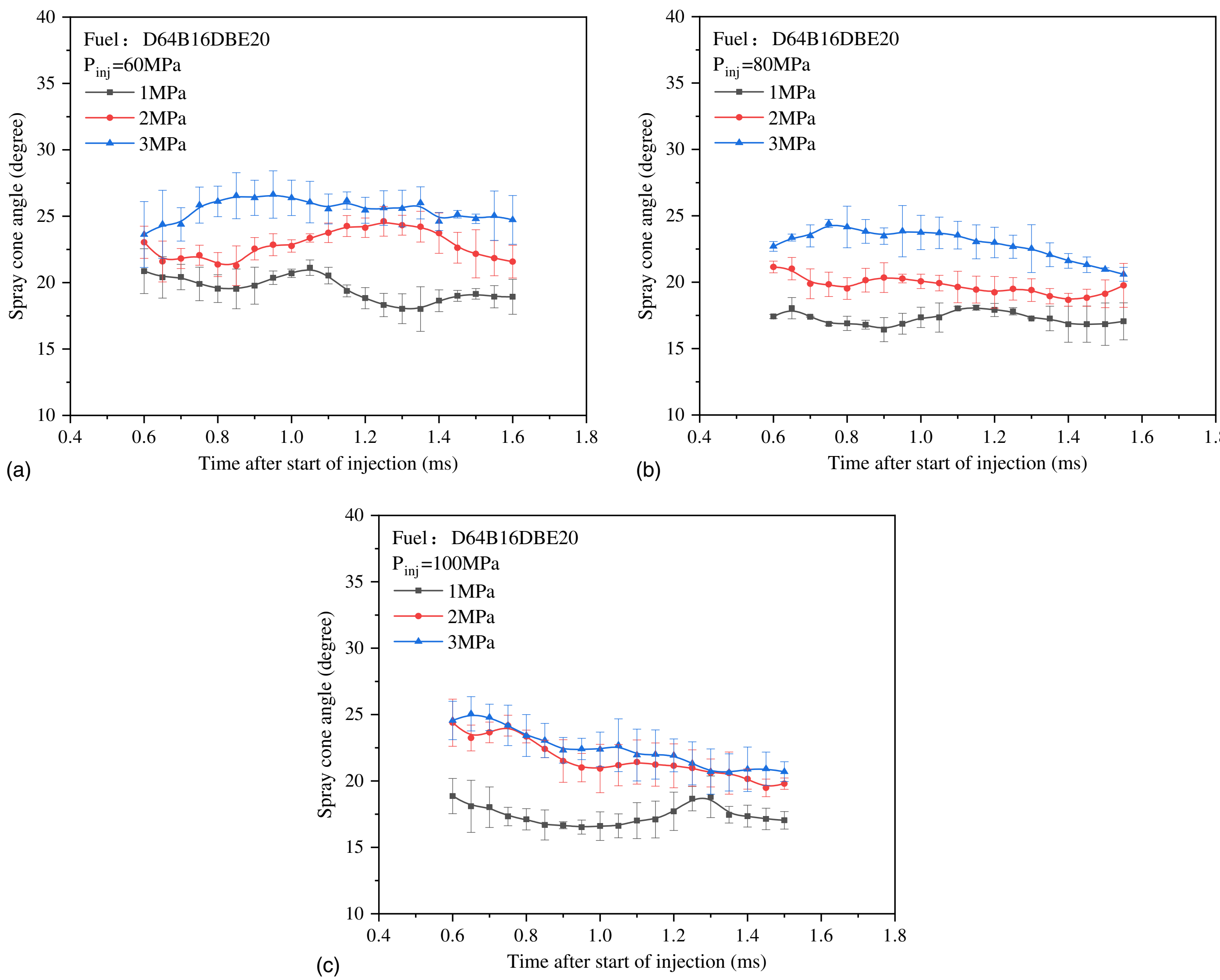

Fig. 11. Effect of ambient pressure on spray cone angle of D64B16DBE20 under injection pressure of (a) 60 MPa; (b) 80 MPa; and (c) 100 MPa.

Results and Discussion

Spray tip penetration and spray cone angle are the two most frequently used parameters for studying the spray macroscopic characteristics of fuels. As shown in Fig. 4, spray tip penetration is defined as the axial distance from the injector nozzle exit to the spray tip; this distance is labeled "S" in the figure. Spray cone angle is defined as the angle between the two lines connecting the nozzle exit point and two periphery points at the position of half penetration. Spray projected area refers to the projected area of the spay perpendicular to the parallel light plane, which corresponds to the shadowed area within the boundary contour in Fig. 4.

Spray Tip Penetration

Fig. 5 presents the temporal evolution of spray tip penetration for the five test fuels at injection pressures of 70, 80, and 90 MPa and corresponding ambient pressures of 3, 2, and 1 MPa, respectively. Under the three conditions, all fuels exhibited a similar penetration development trend: in the initial phase (the primary breakup stage) after the start of injection, all penetrations increased rapidly; after a critical time, the penetration growth slowed down. This can be explained by the fact that the liquid jet initially disintegrates into large ligaments, or droplets, near the nozzle orifice due to the turbulence and cavitation generated inside the injector, and then the jet further breaks into smaller droplets by means of aerodynamic forces in the so-called secondary breakup stage, resulting in a decrease in momentum; therefore, the penetration evolution was retarded. In addition, under the same experimental conditions, the penetration evolution of the different fuels was almost identical in the initial phase due to the similar densities of the test fuels and the similar initial jet velocity caused by the same injection conditions. In the later stage, the differences among the test fuels gradually emerged over time. D80B20 always showed longer penetration length than the other four fuels, and the addition of DBE tended to decelerate the spray penetration evolution. Compared to D80B20, the relative lower density of DBE resulted in a slightly smaller initial momentum. DBE also possesses superior volatility, which enhances cavitation inside the injector and promotes the breakup and atomization processes of the liquid jet. The spray contains more droplets, and its velocity is reduced due to momentum loss. An important factor affecting spray tip penetration is the much lower kinematic viscosity of DBE. The viscosity of the ternary blends decreased with increasing DBE volume in the blended fuel.

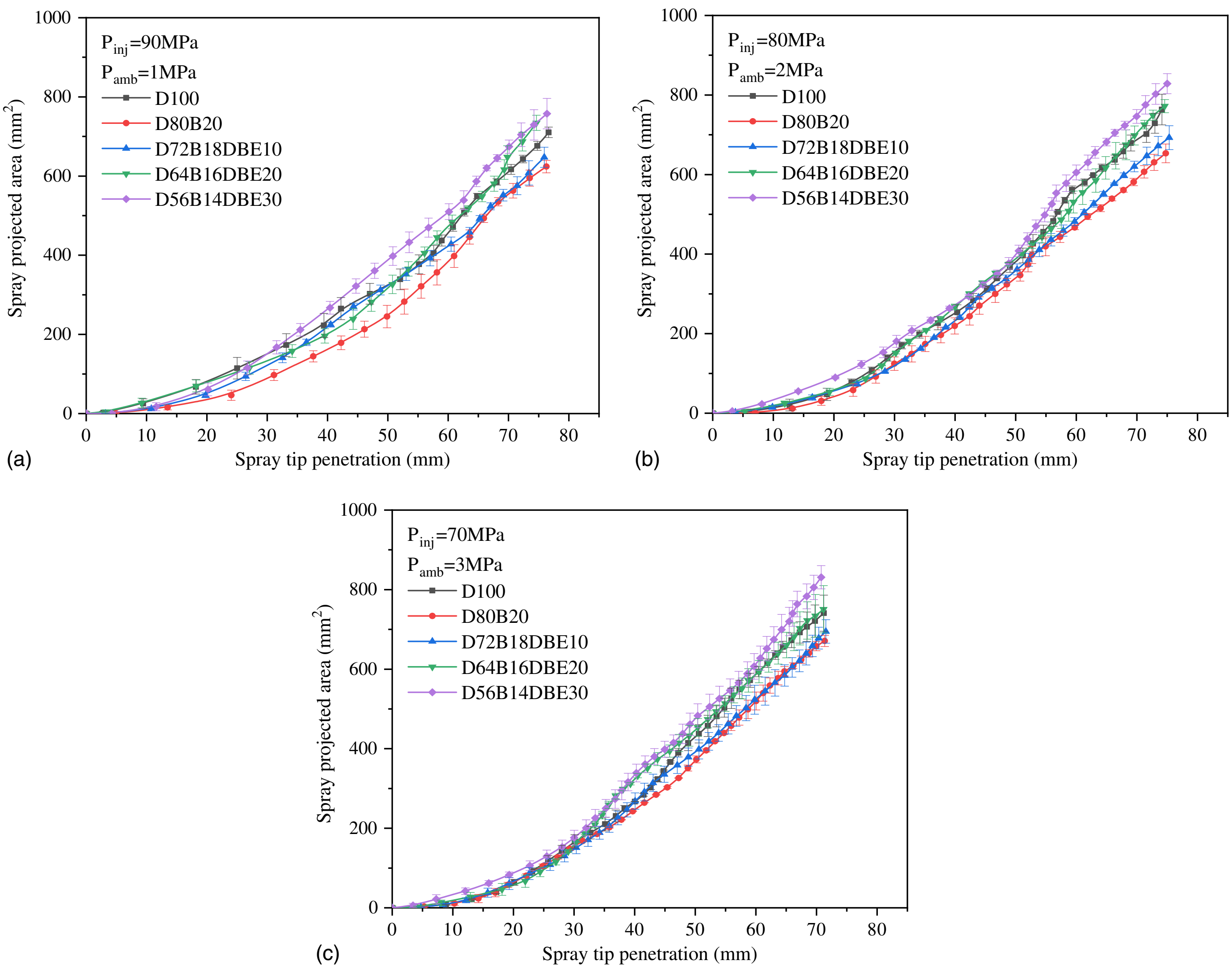

Fig. 12. Spray projected area for diesel and blended fuels under (a) injection pressure of 90 MPa and ambient pressure of 1.0 MPa; (b) injection pressure of 80 MPa and ambient pressure of 2.0 MPa; and (c) injection pressure of 70 MPa and ambient pressure of 3.0 MPa.

Thus, the spray was more susceptible to break up into smaller droplets, causing more momentum to be transferred into the entrained gas, which ultimately led to a slightly shorter penetration length. Overall, although the addition of DBE had no obvious effect on spray tip penetration, it had a tendency to shorten the penetration length. From this trend, it can be judged that there is an optimum blending ratio for improving the spray characteristics. For diesel engines, shorter spray penetration length is conducive to mitigating fuel spray impingement on the piston bowl and cylinder wall, which influences the fuel-air mix as well as combustion and emissions (Luo et al. 2019; Wang et al. 2019). The addition of DBE is expected to promote complete combustion and reduce soot formation to some extent.

It can be seen from the aforementioned three conditions that the 64% diesel–16% biodiesel–20% DBE blend (D64B16DBE20) showed a slightly shorter penetration length than diesel but was the blend with the closest penetration length to that of diesel. In Fig. 6, the effect of injection pressure on the spray tip penetration of D64B16DBE20 is presented. The penetration length gradually increased as the injection pressure rose. This was because the injection pressure directly affected the initial jet velocity and momentum. Higher injection pressure results in higher initial spray tip velocity and accelerates the spray penetration evolution. In addition, with increased injection pressure, the gap of spray tip penetration between adjacent injection pressures becomes smaller. In other words, the effect of injection pressure on spray tip penetration decreases as the injection pressure rises.

Fig. 7 shows the effect of ambient pressure on spray tip penetration evolution for D64B16DBE20. Obviously, in the initial phase, there was little difference in spray tip penetration as the ambient pressure changed. At the near nozzle region, the spray was denser and the penetration was mainly decided by the initial jet velocity. A 1-MPa increase in the ambient pressure was negligible compared to the much higher injection pressure. Therefore, spray tip penetration was not affected that much by ambient conditions; it was mainly dominated by the injection pressure at this stage. Similar results have also been reported in the literature (Jing et al. 2017)—that only slight changes in the dense spray region can be observed by changing the ambient pressure. After a critical time, penetration length decreases significantly as the ambient pressure rises. On the one hand, due to further breakups, the droplets in this so-called diluted spray region are usually finer, resulting in more contact with the surrounding gas, which enhances the influence of the ambient gas resistance force on the spray. Therefore, the penetration is no

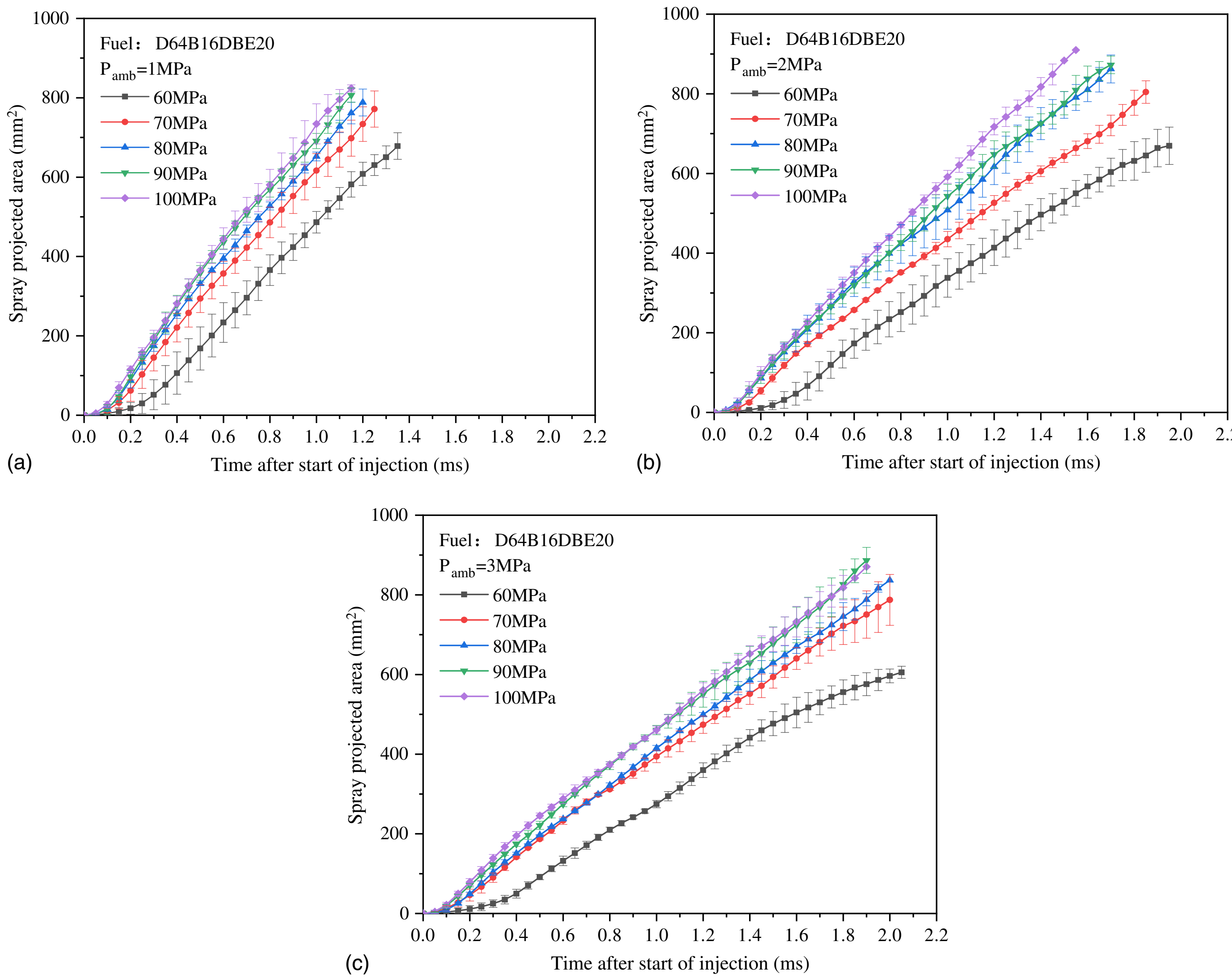

Fig. 13. Effect of injection pressure on spray projected area of D64B16DBE20 under ambient pressure of (a) 1.0 MPa; (b) 2.0 MPa; and (c) 3.0 MPa.

longer determined by the initial jet velocity, and the penetration length no longer depends on the injection pressure. On the other hand, higher ambient density due to increasing ambient pressure strengthens the aerodynamic drag force on the fuel, which inhibits spray axial development. In summary, ambient pressure plays an important role in spray penetration only in the secondary breakup stage.

Spray Cone Angle

Fig. 8 illustrates the spray cone angle of D100, D80B20, a the 72% diesel–18% biodiesel–10% DBE blend (D72B18DBE10), D64B16DBE20, and the 56% diesel–14% biodiesel–30% DBE blend (D56B14DBE30) at an injection pressure of 90 MPa and an ambient pressure of 1 MPa. The spray angle for all test fuels showed a sharp increasing trend after the start of injection. This can be explained by the fact that the radial velocity of the liquid jet drastically changed, and the spray had a blob-like shape at the outset due to the injection needle valve opening and fuel flow inside the nozzle. Subsequently, the cone angle decreased rapidly under the influence of the ambient gas. The effect of fuel type on spray cone angle cannot be clearly compared in such cases. With the evolution of the spray, the fuels gradually achieved a stable flow state after the needle valve was fully opened, and the spray cone angle approached a constant value. Therefore, the time-averaged spray cone angle in the stable fluctuation phase is presented in Fig. 9 to compare the influence of the different fuel types. The results show that D80B20 had the smallest averaged cone angle, and the averaged cone angle of the ternary blends increased with increasing DBE blending ratio in all conditions. Considering the lower viscosity and density of DBE relative to D80B20 (as shown in Table 1), the liquid jet of the ternary blends was more likely to disintegrate into ligaments or droplets, as mentioned previously; this contributed to the spray radial diffusion. In addition, the density of the blends decreased slightly with increasing DBE blending ratio, resulting in a smaller initial momentum, which reduced the ability of the spray to withstand aerodynamic drag; therefore, the spray expanded in the radial direction. A larger spray cone angle contributes to better air entrainment into the spray (Wang et al. 2019), which facilitates the uniformity of the fuel-air mix. Perhaps the addition of DBE can promote the efficient combustion of diesel-biodiesel blends. Furthermore, the averaged cone angle of D64B16DBE20 was similar to that of diesel. Despite the higher viscosity of diesel relative to D72B18DBE10 and D64B16DBE20,

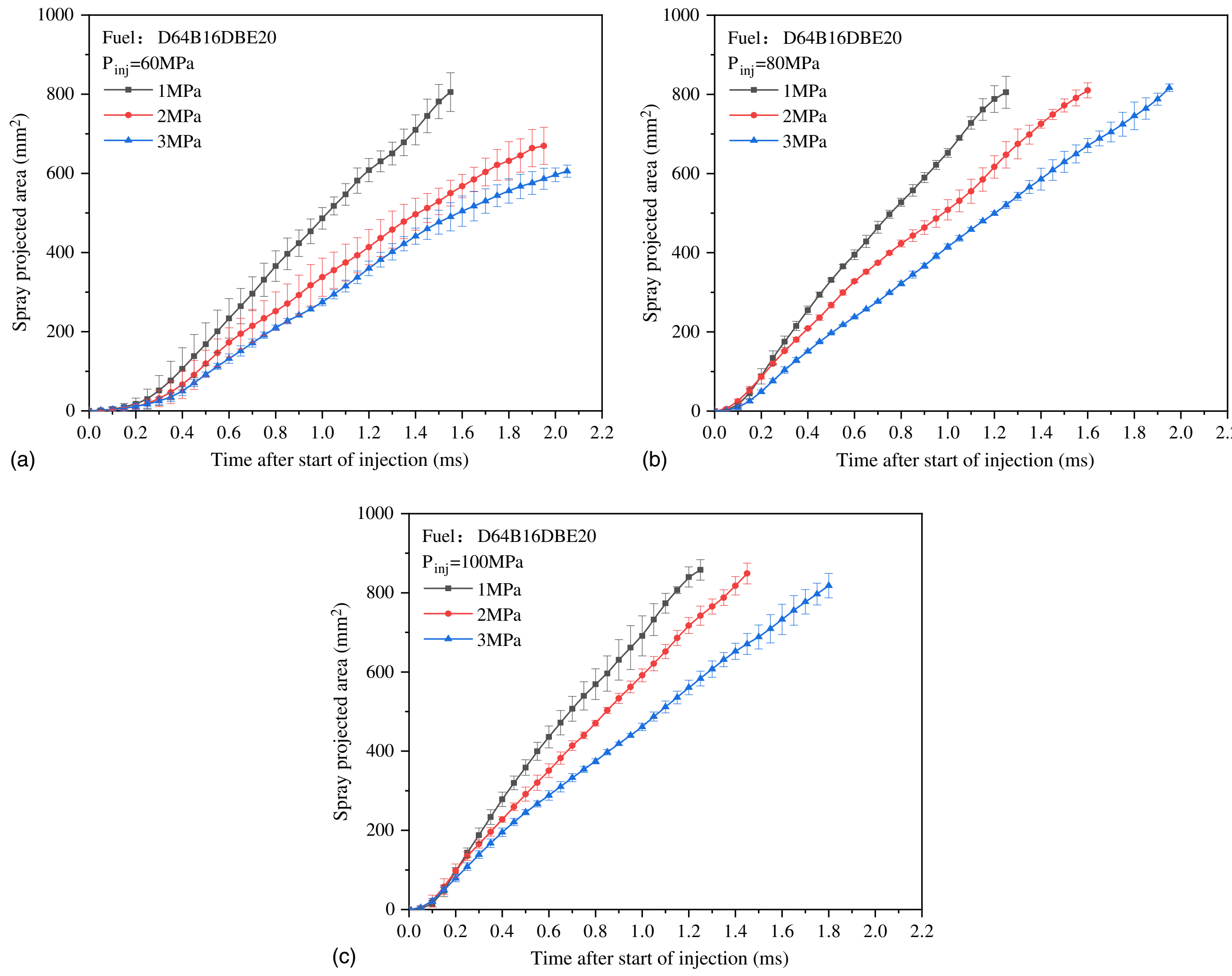

Fig. 14. Effect of ambient pressure on spray projected area of D64B16DBE20 under injection pressure of (a) 60 MPa; (b) 80 MPa; and (c) 100 MPa.

D72B18DBE10 has a higher density and produced a smaller averaged cone angle, while the only slightly higher density of D64B16DBE20 resulted in an averaged angle similar to that of diesel.

Fig. 10 shows the effect of injection pressure on spray cone angle for D64B16DBE20. With decreasing injection pressure, the spray cone angle increased slightly. When the ambient pressure was fixed, the reduced injection pressure provided the spray with less initial momentum and lower kinetic energy, and the spray axial development was restrained to a greater extent by aerodynamic forces; this made it easier for the spray to spread to a larger cone angle. The minimum injection pressure of 60 MPa corresponded to the largest spray cone angle. In general, however, injection pressure has little effect on the spray cone angle (Fu et al. 2017). Fig. 11 shows the variation of spray cone angle along with the ambient pressure. The spray cone angle increased significantly as the ambient pressure rose. In higher density environments, because of greater shear force, the spray breaks up into more droplets that spread around. Moreover, higher ambient pressures increase aerodynamic drag forces, which promote the conversion of spray axial momentum into radial momentum. In conclusion, ambient pressure exerts a dominant effect on spray cone angle, relative to injection pressure.

Spray Projected Area

Spray projected area is a key parameter for the characterization of fuel-air mix behavior. In general, the larger the spray area, the better the fuel-air mixture (Zhan et al. 2018). Better mixing results in a larger quantity of premixed combustion, which inhibits diffusion combustion (Wang et al. 2019). This contributes to more complete combustion. Fig. 12 demonstrates the spray projected area of the five test fuels versus the spray tip penetration at various injection pressures and ambient pressures. Among the five test fuels, D80B20 had the smallest spray projection area. The addition of DBE tended to increase the spray projected area. However, there was little difference between D80B20 and the ternary blend with a DBE volume fraction of 10%. This indicates that adding a small amount (10%) of DBE to DB is not effective in improving the quality of mixture formation. When DBE was blended into DB at a volume fraction of 20%, the spray projected area of the blend was slightly larger than that of D80B20. The blend with 30%

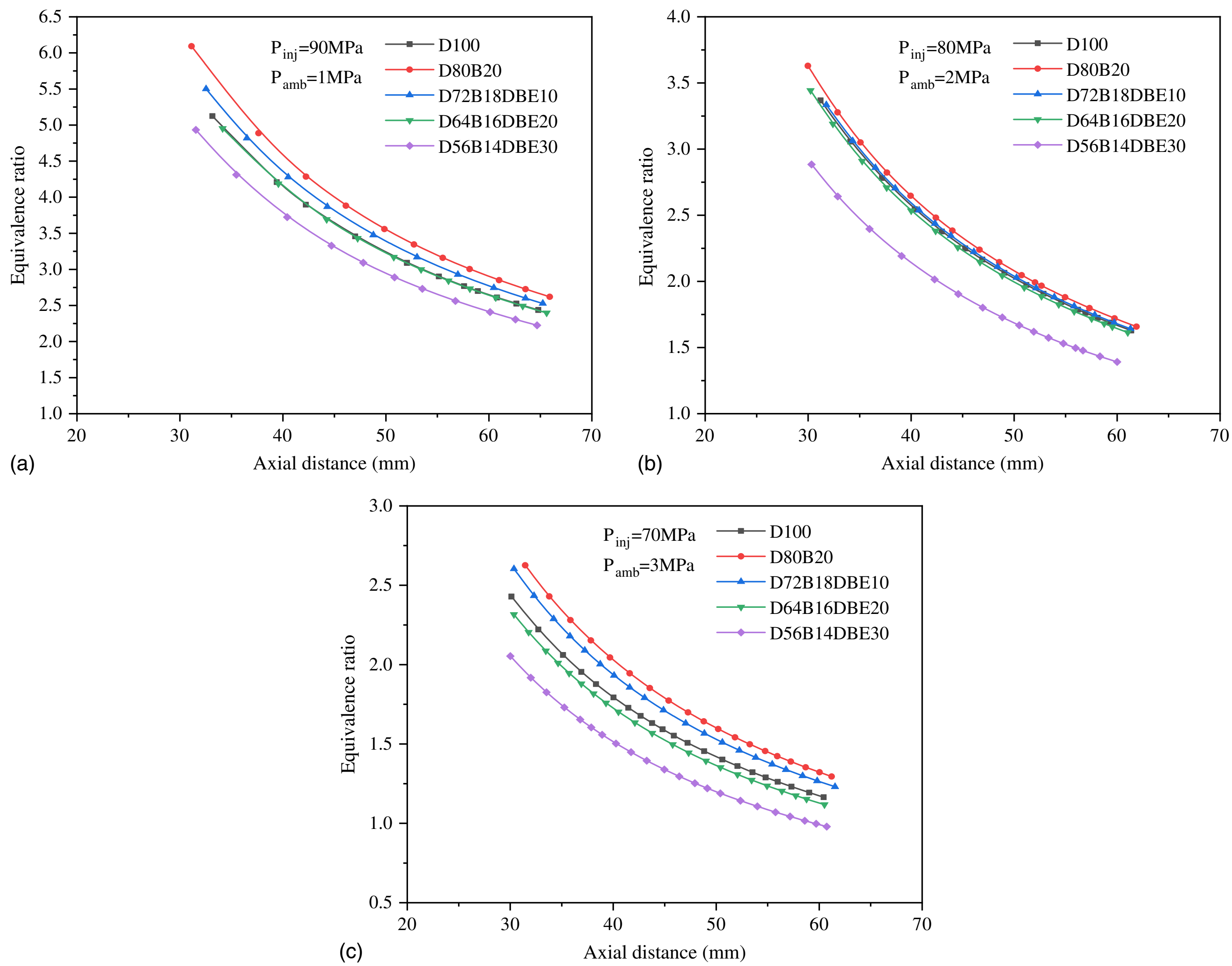

Fig. 15. Averaged cross-sectional equivalence ratio along the injector axis under (a) injection pressure of 90 MPa and ambient pressure of 1.0 MPa; (b) injection pressure of 80 MPa and ambient pressure of 2.0 MPa; and (c) injection pressure of 70 MPa and ambient pressure of 3.0 MPa.

DBE clearly had the largest projected area among the five fuels. Therefore, when the DBE blending ratio is greater than 20%, the addition of DBE enhances the fuel-air mixing process and may improve engine performance through more complete combustion. Spray projection area is directly related to penetration length and cone angle. In this study, although spray penetration length decreased with increasing DBE volume fraction in the blends, the enlarged spray angle led to an increase in spray projected area. Therefore, compared to penetration length, cone angle had a more prominent impact on spray projected area in this experiment. In addition, under three experimental conditions, D64B16DBE20 and diesel had similar spray tip penetration and averaged cone angle distribution, as seen in Figs. 5 and 9, respectively. Therefore, the spray projected area of D64B16DBE20 should be the closest to that of diesel. This is consistent with the experimental data shown in Fig. 12.

Fig. 13 presents the spray projected area versus injection time for D64B16DBE20 and reveals the influence of injection pressure on it. The results show that the spray area increased as the injection pressure rose. As mentioned previously, increased injection pressure produces longer spray penetration length and slightly smaller cone angle. The variation in projected area induced by the injection pressure was in agreement with that of penetration length; this reveals that spray cone angle is insensitive to injection pressure, while the spray tip penetration is visibly affected by it. Fig. 14 shows the effect of ambient pressure on spray projected area for D64B16DBE20. When the injection pressure was fixed and the ambient pressure became large, the spray projected area initially varied little, and then decreased significantly. This was because, although spray cone angle increases with increasing ambient pressure, penetration length is initially almost unaffected by it and then significantly decreases during the secondary breakup stage. In other words, under the combined action of the aforementioned two parameters, the variation trend for spray projection area with ambient pressure was identical to that of penetration length; this indicates that shorter penetration length will lead to smaller projected area when the ambient pressure is increased.

Air Entrainment Analysis

A previous experimental study (Wang et al. 2010) proved that the turbulent jet theory could be employed to study the air entrainment characteristics of liquid fuel jets. Based on this theory, Naber and Siebers (1996) described the following formula

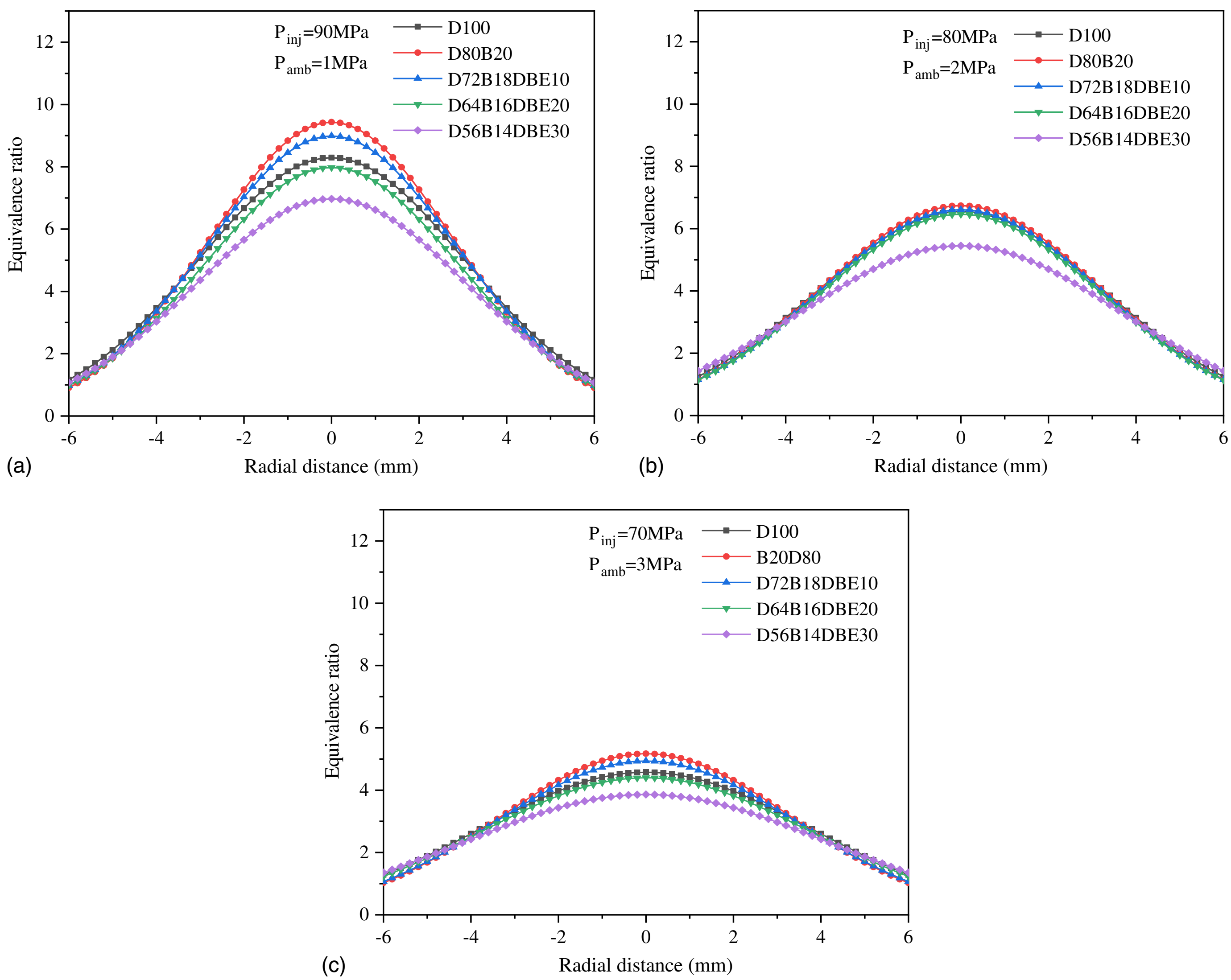

Fig. 16. Radial profiles of equivalence ratio at 40 mm downstream of injector tip under (a) injection pressure of 90 MPa and ambient pressure of 1.0 MPa; (b) injection pressure of 80 MPa and ambient pressure of 2.0 MPa; and (c) injection pressure of 70 MPa and ambient pressure of 3.0 MPa.

for the ratio of air entrainment to the injected fuel at any axial position:

$$\bar{\phi}(x) = \frac{2(A/F)_{st}}{\sqrt{1 + 16(x/x^{+})} - 1} \quad (1)$$

where $\bar{\phi}(x)$ = averaged cross-sectional equivalence ratio at any position along the central axis of the spray; $(A/F)_{st}$ = stoichiometric air:fuel ratio; x = axial distance; and x^{+} = characteristic length scale for a fuel jet and is defined in Eq. (2).

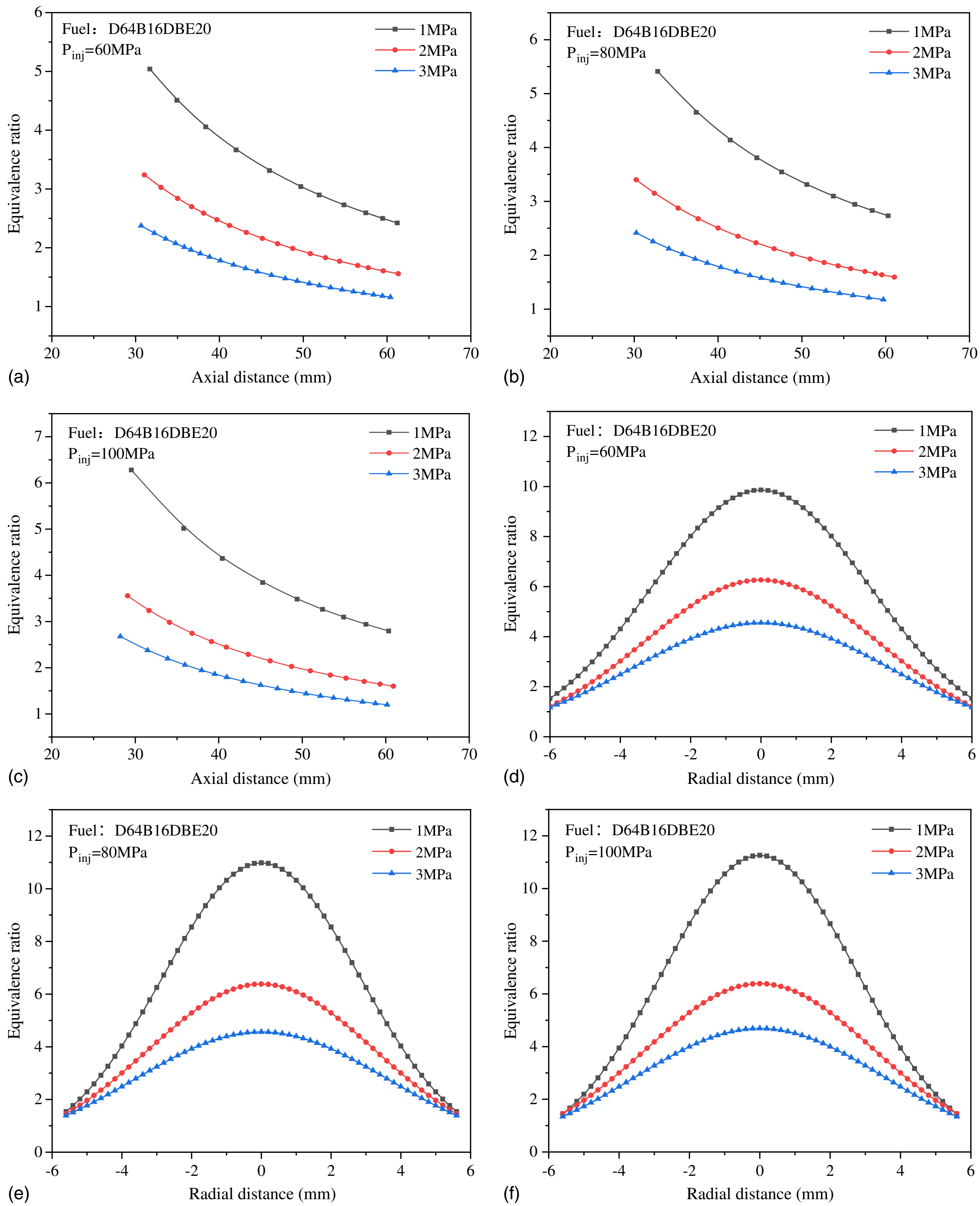

Fig. 17. Effect of ambient pressure on equivalence ratio of D64B16DBE20 under injection pressure of (a) 60 MPa; (b) 80 MPa; and (c) 100 MPa; and effect of ambient pressure on radial equivalence ratio of D64B16DBE20 under injection pressure of (d) 60 MPa; (e) 80 MPa; and (f) 100 MPa.

$$x^+ = \sqrt{\frac{\rho_f}{\rho_a}}\frac{\sqrt{C_a}d_0}{a\tan(\theta/2)} \quad (2)$$

where ρ_f = fuel density; ρ_a = ambient density; C_a = orifice area contraction coefficient, which is assumed to be 0.9 in this study (Zhang et al. 2008); d_0 = orifice diameter; a = a constant with a value of 0.75; and θ = spray cone angle.

Wang et al. (2010) also gave the equivalence ratio over the spray radius for a more complete understanding of spray mixing behavior:

$$\phi(x,r) = 2.55\bar{\phi}(x)\exp\left(-\alpha\left(\frac{r}{R}\right)^2\right) \quad (3)$$

where α = Gaussian distribution shape factor [according to the literature (Fu et al. 2017), its value is 0.23]; $R = r\tan(\theta/2)$; and r = radial distance.

Fig. 15 shows the averaged cross-sectional equivalence ratio at any position along the injector axis for the five test fuels under various conditions. It can be seen that the equivalence ratio is inversely related to the axial distance, which means that more air is entrained as the spray penetrates forward. D80B20 had the largest averaged equivalent ratio and that of the blend decreased as DBE blending ratio increased. This was because the equivalent ratio is related to the stoichiometric air–fuel ratio, spray cone angle, experimental conditions, and the fuel and ambient densities, as shown in Eq. (1). When the experimental conditions were definite, that is, when the ambient pressure, injection pressure, and ambient density are constant, the averaged equivalent ratio along the spray axial direction was mainly dominated by the stoichiometric air:fuel ratio and spray cone angle. The air:fuel ratio of DBE is relatively small due to its oxygen-containing chemical structure; this leads to a lower equivalence ratio. At the same time, the spray cone angle increased as the DBE blending ratio increased. Therefore, the combination of the stoichiometric air:fuel ratio and spray cone angle brought about a decreased equivalent ratio for the blends. Radial profiles of the equivalence ratio at any radial position 40 mm downstream of the injector tip are shown in Fig. 16. D80B20 had the largest and narrowest equivalence ratio, and the addition of DBE to the blends resulted in wider equivalence ratio profiles. This indicates that the addition of DBE can improve the air entrainment and atomization characteristics of diesel-biodiesel blends. From the aforementioned two profiles, it can be seen that D64B16DBE20 and diesel present similar equivalence ratios, which means that these two fuels have comparable air entrainment characteristics and fuel-air mixture formation. This may make D64B16DBE20 as good as diesel in terms of combustion characteristics, performance, and emissions. In addition, as shown in Fig. 17, the equivalence ratio of D64B16DBE20 decreased significantly when the ambient pressure increased. Due to the higher ambient density, the spray cone angle increased and penetration became slower, causing more air to be entrained by fuel.

Conclusions

In this study, the effects of DBE blending ratio, injection pressure, and ambient pressure on spray characteristics were experimentally investigated using a high-speed photography method. The conclusions, based on the experimental results, are as follows:

1. D80B20 had the longest spray penetration length, the smallest spray cone angle, and the smallest projected area among the five test fuels. With increased DBE volume fraction (tested up to 30% in the present study) in the diesel-biodiesel-DBE ternary blends, spray tip penetration tended to decrease, the equivalence ratio decreased, and the spray cone angle and the spray projected area increased.
2. With increased injection pressure, the spray tip penetration and projected area of D64B16DBE20 increased; spray cone angle was less influenced.
3. With increased ambient pressure, spray tip penetration, projected area, and equivalence ratio decreased, but spray cone angle increased significantly. Ambient pressure played an important role in changing spray tip penetration only in the secondary breakup stage.
4. The addition of DBE can improve the air entrainment characteristics of DB; this is expected to promote complete combustion and reduce soot formation to some extent. D64B16DBE20 and diesel present comparable equivalence ratios and spray characteristics, such as spray tip penetration, cone angle, and projected area, indicating that D64B16DBE20 can be used in a diesel engine without any engine modifications.

Acknowledgments

This work was supported by the National Natural Science Foundation of China (Grant Nos. 51376171 and 11372303) and the Doctoral Foundation of Southwest University of Science and Technology (Grant No. 18zx7164).

References

Akgün, N., and E. İşcan. 2007. "Effects of process variables for biodiesel production by transesterification." *Eur. J. Lipid Sci. Technol.* 109 (5): 486–492. https://doi.org/10.1002/ejlt.200600210.

Beeckmann, J., M. M. Aye, R. Gehmlich, and N. Peters. 2010. *Experimental investigation of the spray characteristics of di-n-butyl ether (DNBE) as an oxygenated compound in diesel fuel*. SAE Technical Paper 2010-01-1502. Warrendale, PA: SAE International.

Belgiorno, G., G. Di Blasio, S. Shamun, C. Beatrice, P. Tunestål, and M. Tunér. 2018. "Performance and emissions of diesel-gasoline-ethanol blends in a light duty compression ignition engine." *Fuel* 217 (Apr): 78–90. https://doi.org/10.1016/j.fuel.2017.12.090.

Bi, S., G. Zhao, and J. Wu. 2009. "Surface tension of diethyl ether, diisopropyl ether, and dibutyl ether." *J. Chem. Eng. Data* 55 (4): 1523–1526. https://doi.org/10.1021/je900665a.

Boggavarapu, P., and R. Ravikrishna. 2013. "A review on atomization and sprays of biofuels for IC engine applications." *Int. J. Spray Combust. Dyn.* 5 (2): 85–121. https://doi.org/10.1260/1756-8277.5.2.85.

BP (British Petroleum). 2017. "BP statistical review of world energy June 2017." Accessed September 12, 2018. http://www.bp.com/en/global/corporate/energy-economics/statistical-review-of-world-energy.html.

Coram, A., and D. W. Katzner. 2018. "Reducing fossil-fuel emissions: Dynamic paths for alternative energy-producing technologies." *Energy Econ.* 70 (Feb): 179–189. https://doi.org/10.1016/j.eneco.2017.12.028.

Das, M., M. Sarkar, A. Datta, and A. K. Santra. 2018. "Study on viscosity and surface tension properties of biodiesel-diesel blends and their effects on spray parameters for CI engines." *Fuel* 220 (May): 769–779. https://doi.org/10.1016/j.fuel.2018.02.021.

Dhar, A., and A. K. Agarwal. 2014. "Performance, emissions and combustion characteristics of Karanja biodiesel in a transportation engine." *Fuel* 119 (Mar): 70–80. https://doi.org/10.1016/j.fuel.2013.11.002.

Dhar, A., R. Kevin, and A. K. Agarwal. 2012. "Production of biodiesel from high-FFA neem oil and its performance, emission and combustion characterization in a single cylinder DICI engine." *Fuel Process. Technol.* 97 (May): 118–129. https://doi.org/10.1016/j.fuproc.2012.01.012.

Fu, W., L. Song, T. Liu, and Q. Lin. 2017. "Experimental study of spray characteristics of biodiesel blending with diethyl carbonate in a common rail injection system." *Proc. Inst. Mech. Eng. Part D: J.*

Autom. Eng. 233 (2): 249–262. https://doi.org/10.1177/0954407017740792.

Gebremariam, S. N., and J. M. Marchetti. 2018. "Economics of biodiesel production: Review." *Energy Convers. Manage.* 168 (Jul): 74–84. https://doi.org/10.1016/j.enconman.2018.05.002.

Guan, L., C. Tang, K. Yang, J. Mo, and Z. Huang. 2015. "Effect of di-n-butyl ether blending with soybean-biodiesel on spray and atomization characteristics in a common-rail fuel injection system." *Fuel* 140 (Jan): 116–125. https://doi.org/10.1016/j.fuel.2014.09.104.

Heuser, B., P. Mauermann, R. Wankhade, F. Kremer, and S. Pischinger. 2015. "Combustion and emission behavior of linear C8-oxygenates." *Int. J. Engine Res.* 16 (5): 627–638. https://doi.org/10.1177/1468087415594951.

Huang, D., H. Zhou, and L. Lin. 2012. "Biodiesel: An alternative to conventional fuel." *Energy Procedia* 16 (Part C): 1874–1885. https://doi.org/10.1016/j.egypro.2012.01.287.

Jing, D., F. Zhang, Y. Li, H. Xu, and S. Shuai. 2017. "Experimental investigation on the macroscopic and microscopic spray characteristics of dieseline fuel." *Fuel* 199 (Jul): 478–487. https://doi.org/10.1016/j.fuel.2017.02.055.

Knothe, G., and L. F. Razon. 2017. "Biodiesel fuels." *Prog. Energy Combust. Sci.* 58 (Jan): 36–59. https://doi.org/10.1016/j.pecs.2016.08.001.

Krishnan, V., L. Gonzalez-Marciaga, and J. McCalley. 2014. "A planning model to assess hydrogen as an alternative fuel for national light-duty vehicle portfolio." *Energy* 73 (Aug): 943–957. https://doi.org/10.1016/j.energy.2014.06.109.

Lapuerta, M., O. Armas, and J. Rodriguezfernandez. 2008. "Effect of biodiesel fuels on diesel engine emissions." *Prog. Energy Combust. Sci.* 34 (2): 198–223. https://doi.org/10.1016/j.pecs.2007.07.001.

Li, F., B. Yi, W. Fu, L. Song, T. Liu, H. Hu, and Q. Lin. 2017. "Experimental study on spray characteristics of long-chain alcohol-diesel fuels in a constant volume chamber." *J. Energy Inst.* 92 (1): 94–107. https://doi.org/10.1016/j.joei.2017.11.002.

Luo, H., K. Nishida, Y. Ogata, W. Zhang, and T. Fujikawa. 2019. "Fuel adhesion characteristics under non-evaporation and evaporation conditions. Part 1: Effect of injection pressure." *Fuel* 240 (Mar): 317–325. https://doi.org/10.1016/j.fuel.2018.12.004.

Meng, X., J. Wu, and Z. Liu. 2008. "Viscosity and density measurements of diisopropyl ether and dibutyl ether at different temperatures and pressures." *J. Chem. Eng. Data* 54 (9): 2353–2358. https://doi.org/10.1021/je8005369.

Miyamoto, N., H. Ogawa, and M. Nabi. 2000. "Approaches to extremely low emissions and efficient diesel combustion with oxygenated fuels." *Int. J. Engine Res.* 1 (1): 71–85. https://doi.org/10.1243/1468087001545272.

Naber, J. D., and D. L. Siebers. 1996. "Effects of gas density and vaporization on penetration and dispersion of diesel sprays." In *SAE 1984 transactions*, 82–111. Warrendale, PA: SAE International.

Park, S. H., and C. S. Lee. 2013. "Combustion performance and emission reduction characteristics of automotive DME engine system." *Prog. Energy Combust. Sci.* 39 (1): 147–168. https://doi.org/10.1016/j.pecs.2012.10.002.

Park, Y., J. Hwang, C. Bae, K. Kim, J. Lee, and S. Pyo. 2015. "Effects of diesel fuel temperature on fuel flow and spray characteristics." *Fuel* 162 (Dec): 1–7. https://doi.org/10.1016/j.fuel.2015.09.008.

Sajjad, H., H. Masjuki, M. Varman, M. Kalam, M. Arbab, S. Imtenan, and S. A. Rahman. 2014. "Engine combustion, performance and emission characteristics of gas to liquid (GTL) fuels and its blends with diesel and bio-diesel." *Renewable Sustainable Energy Rev.* 30 (Feb): 961–986. https://doi.org/10.1016/j.rser.2013.11.039.

Shamun, S., G. Belgiorno, G. Di Blasio, C. Beatrice, M. Tunér, and P. Tunestål. 2018. "Performance and emissions of diesel-biodiesel-ethanol blends in a light duty compression ignition engine." *Appl. Therm. Eng.* 145 (Dec): 444–452. https://doi.org/10.1016/j.applthermaleng.2018.09.067.

Suresh, M., C. P. Jawahar, and A. Richard. 2018. "A review on biodiesel production, combustion, performance, and emission characteristics of non-edible oils in variable compression ratio diesel engine using biodiesel and its blends." *Renewable Sustainable Energy Rev.* 92 (Sep): 38–49. https://doi.org/10.1016/j.rser.2018.04.048.

Szybist, J. P., A. D. Youngquist, T. L. Barone, J. M. Storey, W. R. Moore, M. Foster, and K. Confer. 2011. "Ethanol blends and engine operating strategy effects on light-duty spark-ignition engine particle emissions." *Energy Fuels* 25 (11): 4977–4985. https://doi.org/10.1021/ef201127y.

Vardy, M., M. Oppenheimer, N. K. Dubash, J. O'Reilly, and D. Jamieson. 2017. "The intergovernmental panel on climate change: Challenges and opportunities." *Ann. Rev. Environ. Resour.* 42 (1): 55–75. https://doi.org/10.1146/annurev-environ-102016-061053.

Wang, C., A. Sahu, C. Coratella, C. Xu, J. Saul, and H. Xu. 2019. "Spray characteristics of a gasoline-diesel blend (ULG75) using high-speed imaging techniques." *Fuel* 239 (Mar): 677–692. https://doi.org/10.1016/j.fuel.2018.10.135.

Wang, X., Z. Huang, O. A. Kuti, W. Zhang, and K. Nishida. 2010. "Experimental and analytical study on biodiesel and diesel spray characteristics under ultra-high injection pressure." *Int. J. Heat Fluid Flow* 31 (4): 659–666. https://doi.org/10.1016/j.ijheatfluidflow.2010.03.006.

Wang, Z., S. Wu, Y. Huang, S. Huang, S. Shi, X. Cheng, and R. Huang. 2018. "Experimental investigation on spray, evaporation and combustion characteristics of ethanol-diesel, water-emulsified diesel and neat diesel fuels." *Fuel* 231 (Nov): 438–448. https://doi.org/10.1016/j.fuel.2018.05.129.

Wullenkord, J., L.-S. Tran, J. Böttchers, I. Graf, and K. Kohse-Höinghaus. 2018. "A laminar flame study on di-n-butyl ether as a potential biofuel candidate." *Combust. Flame* 190: 36–49. https://doi.org/10.1016/j.combustflame.2017.11.006.

Xie, H., L. Song, Y. Xie, D. Pi, C. Shao, and Q. Lin. 2015. "An experimental study on the macroscopic spray characteristics of biodiesel and diesel in a constant volume chamber." *Energies* 8 (6): 5952–5972. https://doi.org/10.3390/en8065952.

Yi, B., Q. Lin, L. Song, W. Fu, F. Li, and T. Liu. 2017. "Spray characteristics of n-butanol in a high-pressure common-rail injection system." *J. Energy Eng.* 143 (5): 04017044. https://doi.org/10.1061/(ASCE)EY.1943-7897.0000474.

Zare, A., T. A. Bodisco, M. N. Nabi, F. M. Hossain, Z. D. Ristovski, and R. J. Brown. 2018. "A comparative investigation into cold-start and hot-start operation of diesel engine performance with oxygenated fuels during transient and steady-state operation." *Fuel* 228 (Sep): 390–404. https://doi.org/10.1016/j.fuel.2018.05.004.

Zhan, C., Z. Feng, M. Zhang, C. Tang, and Z. Huang. 2018. "Experimental investigation on effect of ethanol and di-ethyl ether addition on the spray characteristics of diesel/biodiesel blends under high injection pressure." *Fuel* 218 (Apr): 1–11. https://doi.org/10.1016/j.fuel.2017.12.038.

Zhang, W., K. Nishida, J. Gao, and D. Miura. 2008. "An experimental study on flat-wall-impinging spray of microhole nozzles under ultra-high injection pressures." *Proc. Inst. Mech. Eng. Part D: J. Autom. Eng.* 222 (9): 1731–1741. https://doi.org/10.1243/09544070JAUTO858.

Zhen, X., and Y. Wang. 2015. "An overview of methanol as an internal combustion engine fuel." *Renewable Sustainable Energy Rev.* 52 (Dec): 477–493. https://doi.org/10.1016/j.rser.2015.07.083.